

Supporting Information

Shear Adhesion of Tapered Nanopillar Arrays

Younghyun Cho,^{†,§} Helen K. Minsky,[‡] Yijie Jiang,[‡] Kaiyang Yin,[†] Kevin T. Turner,^{*,‡}
and Shu Yang^{*,†}

[†]Department of Materials Science and Engineering, University of Pennsylvania, 3231 Walnut Street, Philadelphia, Pennsylvania 19104, United States

[‡]Department of Mechanical Engineering and Applied Mechanics, University of Pennsylvania, 220 South 33rd Street, Philadelphia, Pennsylvania, 19104, United States

[§]Energy Efficiency and Materials Research Division, Korea Institute of Energy Research, 152 Gajeong-ro, Yuseong-gu, Daejeon, 305-343, Republic of Korea

Corresponding Authors

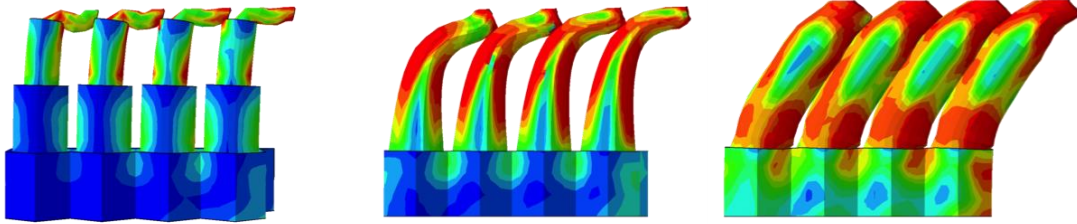
*(S.Y.) E-mail: shuyang@seas.upenn.edu

*(K.T.T.) Email: kturner@seas.upenn.edu

Author Contributions

Y. C. and H.M. contributed equally to this work.

Table S1. Contact area between four neighboring nanopillars from different shaped nanopillars predicted by FE simulation.



Indentation Depth	Contact Area (μm^2)		
	Stepwise	Cone-Shaped	Pencil-like
100 nm	-	-	-
300 nm	0.020	0.044	0.165
400 nm	0.030	0.059	0.259

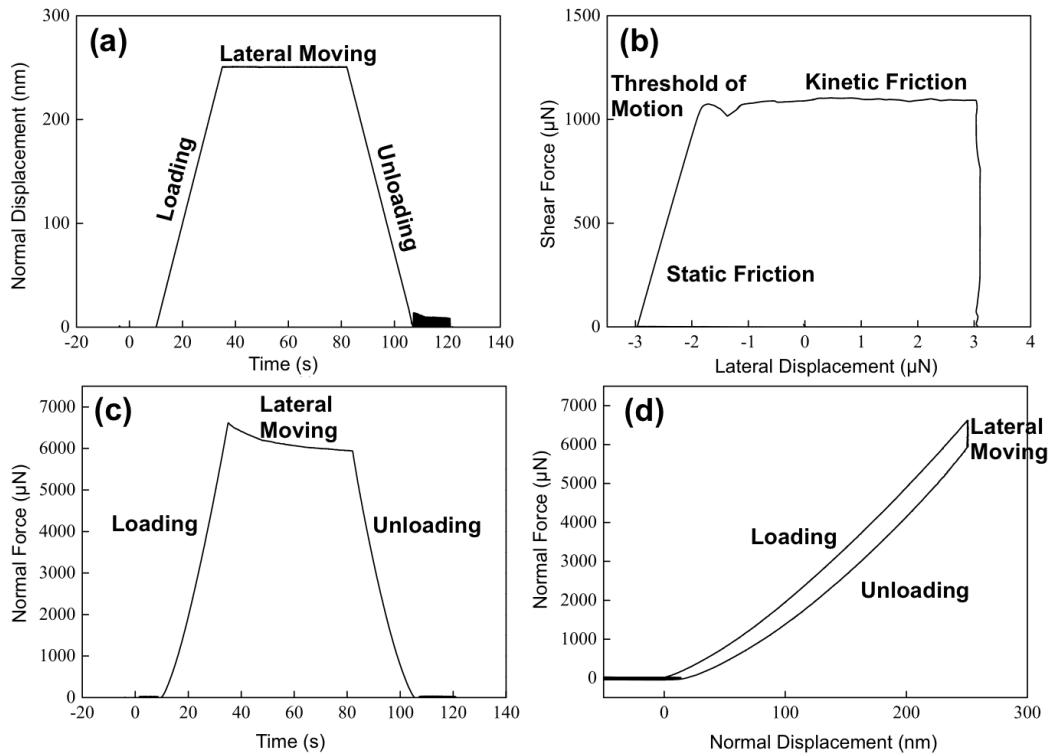


Figure S1. Various curves obtained from bulk epoxy sample during nanoindentation. (a) Normal displacement vs. time, (b) shear force vs. lateral displacement, (c) normal force vs. time, and (d) normal force vs. normal displacement.

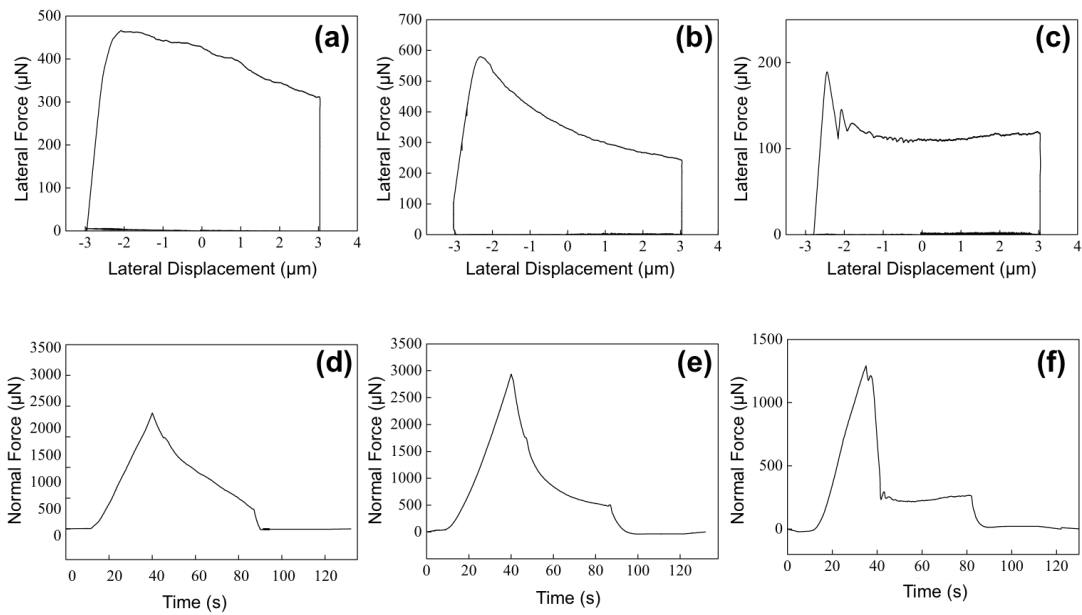


Figure S2. Variation in lateral (a-c) and normal (d-f) forces during sliding of the indenter tip on various nanopillar arrays at an indentation depth of 400 nm. (a) and (d) are for cone-shaped, (b) and (e) are for pencil-like, (c) and (f) are for stepwise nanopillars.

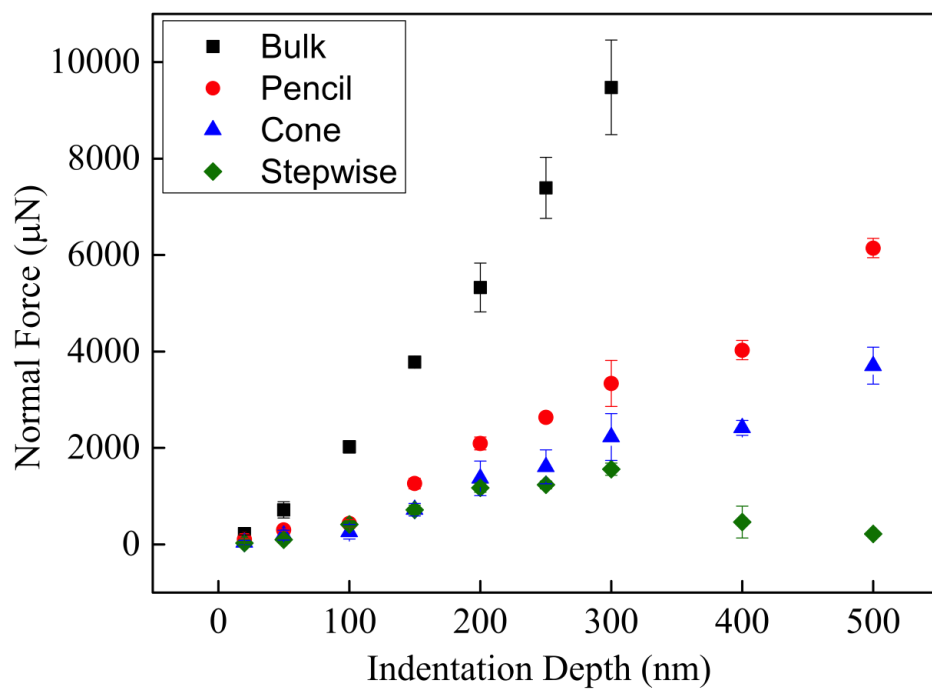


Figure S3. Normal force between the tapered epoxy nanopillar arrays and the nanoindenter tip as a function of the indentation depth using a cono-spherical diamond tip with a nominal radius of 100 μm .

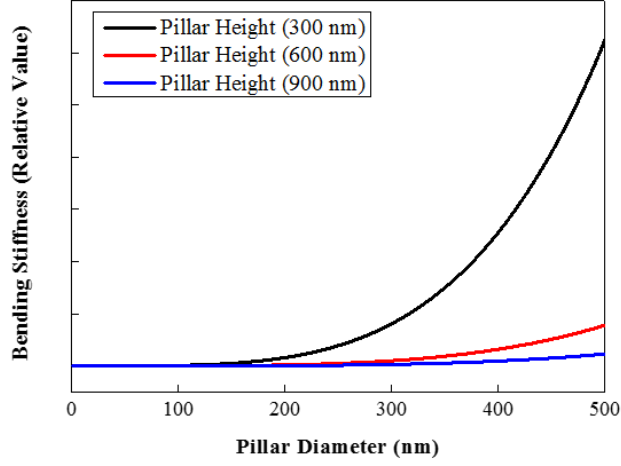


Figure S4. General trend of the relative bending stiffness vs. pillar diameter at various pillar heights.

Figure S4 was plotted based on the calculation viewing the pillar as a cylindrical cantilever beam with a fixed end. The bending stiffness (or elastic restoring force) of an individual nanopillar, F_E , is given by

$$F_E = \frac{3EI\delta}{h^3} \quad (1)$$

And the moment of inertia for a round solid section, I , is given by

$$I = \frac{\pi d^4}{64} \quad (2)$$

where E is the Young's modulus of the pillar material, δ is the deflection, and h is the height of the pillar, and d is the diameter of the pillar, respectively.¹⁻³

Bending stiffness was calculated as a function of pillar diameter at different pillar heights. This value shows the trend of bending stiffness at a different pillar geometry in cylindrical shape.

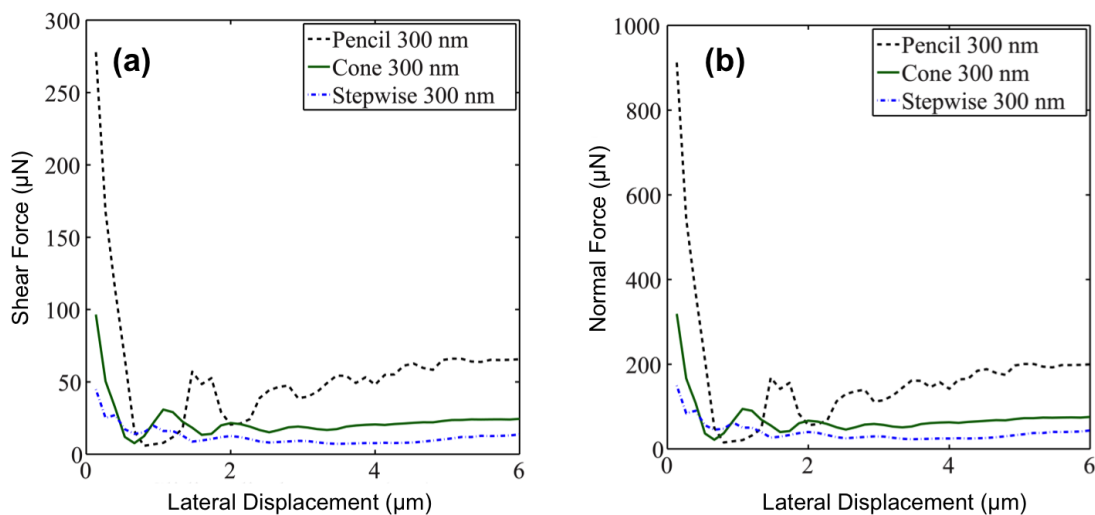


Figure S5. Simulated (a) shear adhesion force and (b) normal forces of various nanopillars as a function of lateral displacement at the indentation depth of 300 nm.

Reference:

- (1) Chandra, D.; Yang, S. Capillary-force-induced clustering of micropillar arrays: is it caused by isolated capillary bridges or by the lateral capillary meniscus interaction force? *Langmuir* **2009**, *25*, 10430-10434.
- (2) Yoon, H.; Kwak, M. K.; Kim, S. M.; Sung, S. H.; Lim, J.; Suh, H. S.; Suh, K. Y.; Char, K. Polymeric nanopillars reinforced with metallic shells in the lower stem region. *Small* **2011**, *7*, 3005-3010.
- (3) Chandra, D.; Yang, S. Stability of High Aspect Ratio Micropillar Arrays against Adhesive and Capillary Forces. *Acc. Chem. Res.* **2010**, *43*, 1080-1091.